Effect of the Pump-Beam Profile and Wavefront on the Amplified Signal Wavefront in Optical Parametric Amplifiers

S.-W. Bahk, I. A. Begishev, R. G. Roides, C. Mileham, R. Cuffney, C. Feng, B. M. Webb, C. Jeon, M. Spilatro, S. Bucht, C. Dorrer, and J. Bromage

Laboratory for Laser Energetics, University of Rochester

Optical parametric chirped-pulse amplification (OPCPA) is known to have advantages over conventional chirped-pulse amplification based on population inversion gain medium.[1] The bandwidth can be extended more than 100 nm without being limited by gain narrowing. The angle between pump and signal beams can be adjusted to provide an even-broader gain bandwidth than collinear geometry. The thermal effect is minimal due to instantaneous energy transfer from pump to signal. The temporal contrast is, in general, better because fewer amplifiers are required and the parametric fluorescence is confined within the pump pulse duration. The OPCPA scheme is a practical way to amplify ultra-broadband pulses to kilojoule energies using commercially available large potassium dihydrogen phosphate (KDP) crystals and existing high-energy nanosecond driver lasers in laser fusion facilities.[2] Deuterated potassium dihydrogen phosphate (DKDP)-based OPCPA systems have been demonstrated on the PEARL laser at the Institute of Applied Physics in Russia[3] and LLE's Multi-Terawatt optical parametric amplifier line (MTW-OPAL).[4] OPCPA lasers based on lithium triborate (LBO)[5,6] or yttrium calcium oxyborate (YCOB)[7] crystals show promising performance at the 800-nm central wavelength seeded by a Ti:sapphire oscillator.

The amplified signal intensity in an optical parametric amplifier (OPA) is a nonlinear function of pump intensity. In general, a flattop pump profile at a fixed intensity is optimal for good conversion efficiency from the pump to signal. In this regime, the amplified signal-beam profile and spectrum are saturated following the pump-beam profile and the pulse shape. The amplification-induced signal phase or "OPA phase" exhibits a phase shift similar to the one observed in a population inversion system.[8] Several authors have investigated the effect of pump on the OPA phase. Ross *et al.* concluded that the OPA phase is a function of pump intensity. They have formally shown that the pump-beam phase impacts the idler phase but does not affect the signal phase.[9] Li *et al.* have experimentally shown that astigmatism in the pump beam is transferred to the idler beam.[10]

Others, however, found that the OPA phase is affected by the pump phase as well. Wei *et al.* have numerically shown that the pump-beam walk-off introduces phase transfer from pump to signal and suggested a walk-off–compensated geometry to mitigate this effect.[11] The same group later experimentally demonstrated the mitigation effect.[12] Chen *et al.* gave a qualitative description of the pump-to-signal phase transfer effect being proportional to the pump wavefront derivative.[13]

Authors in Refs. 10–13 studied the effect of input beam wavefronts on the OPA phase using wave equations and numerical simulations. We analyze this effect using the analytic OPA phase solution and the wave-vector picture. The phase solutions of the three waves in an OPA process have been studied by several researchers[9,14] and were recently presented in closed form in Ref. 15. The main results for the case of zero idler input are summarized here for convenience:

$$\phi_{\mathrm{s}}(L)=\phi_{\mathrm{s}}(0)+\psi_{\mathrm{s}}\left[\Delta k, I_{\mathrm{s}}(0), I_{\mathrm{p}}(0), L\right], \tag{1}$$

$$\phi_{\mathrm{i}}(L)=\pi/2-\phi_{\mathrm{s}}(0)+\phi_{\mathrm{p}}(0)-\Delta k L/2. \tag{2}$$

The function ψ_s is an additional phase introduced in the signal beam by the OPA process and will be equivalently called the "OPA phase." The ψ_s is a function determined by four independent parameters and has a term made of the incomplete elliptic integral of the third kind [for the detailed expression of ψ_s, refer to Eq. (17) of Ref. 15]. I and ϕ denote intensity and phase with the subscripts "s, i, p" indicating signal, idler, and pump, respectively; L is the crystal thickness. The OPA phase is determined by the input signal and pump intensities, the wave-vector mismatch (Δk), and the crystal thickness (L). The dependence on the input signal's intensity is weak for the normal OPA regime, where $I_s(0) \ll I_p(0)$.

Equation (2) shows that the phases of the input signal [$\phi_s(0)$] and input pump [$\phi_p(0)$] are all directly transferred to the output idler phase. Although this is mostly true, the OPA phase ψ_s is not entirely immune to input phase aberrations. The subtlety lies in the fact that the wave vector is normal to the input phase front in a spatially coherent beam; therefore, the spatial phase variation is accompanied by variation in Δk, which in turn impacts ψ_s. (We assume here a regime where diffraction is negligible over the length of the crystal.) The OPA phase also depends on the input pump intensity independently from the input phase.

The OPA phase is linear with respect to Δk within amplification bandwidth. The OPA phase in the linear regime can be approximated as

$$\psi_s \sim -\frac{\Delta k}{2} L \left\{ 1 - \frac{1}{a\sqrt{I_p(0)L}} \tanh\left[a\sqrt{I_p(0)L}\right] \right\}, \tag{3}$$

where $a\left(d_{\mathrm{eff}}/c\right)\sqrt{2\eta_0 \omega_s \omega_i / n_s n_i n_p}$ (Ref. 15). One can numerically show that $a\sqrt{I_p(0)}L \sim 1.16 \log_{10}(\mathrm{gain}) + 1.36$ in the depletion regime with perfect phase matching, where gain is defined as the ratio of output to input signal intensities [$I_s(L)/I_s(0)$]. For a 20-dB gain, $a\sqrt{I_p(0)}L \sim 3.68$, and Eq. (3) in terms of relative phase can be further approximated to

$$\Delta\psi_s \sim -0.36\Delta(\Delta k)L. \tag{4}$$

The local wave vectors of pump and signal waves are normal to their phase front. The wave-vector mismatch is a function of pump and signal phase slopes or derivatives. $\Delta(\Delta k)$ can be written as

$$\Delta(\Delta k) = \left(-\rho_{p,x} + \frac{k_{s,0}}{n_i k_{i,0}} a_{x,0}\right)\frac{\partial \phi_{p,0}}{\partial x} + \left(-\frac{k_{p,0}}{n_i k_{i,0}} a_{x,0}\right)\frac{\partial \phi_{s,0}}{\partial x} + \left(\frac{k_{s,0}}{n_i k_{i,0}} a_{y,0}\right)\frac{\partial \phi_{p,0}}{\partial y} + \left(-\frac{k_{p,0}}{n_i k_{i,0}} a_{y,0}\right)\frac{\partial \phi_{s,0}}{\partial y}. \tag{5}$$

The Δ notation in the above equations denotes relative change across two points in space. The incident pump and signal phase terms here are residual phases that do not include tilt terms corresponding to the incidence angles. Equation (5) shows that the noncollinear interaction angle allows both seed and pump-beam wavefront gradients to be transferred to the OPA phase. On the other hand, the birefringence term ($\rho_{p,x}$) always enables the pump wavefront transfer-to-OPA phase even with the collinear geometry. It is possible to mitigate the birefringence-induced OPA phase by choosing the sign of the noncollinear angle in order to cancel the coefficient of the pump phase gradient, which is the first term in Eq. (5). This was attempted by Wei and Yuan,[11,12] but the cancellation of the pump gradient term increases the signal gradient term, only shifting the problem from the pump to the signal side. Such cancellation is also a trade-off with other considerations that typically constrain the relative angle between pump and signal, e.g., bandwidth requirements and mitigation of parasitic second-harmonic generation.

Equations (4) and (5) show good agreement with the wave-equation approach of Refs. 10–13 in the absence of diffraction except that the small spatial positions shift in the beams coming from birefringence and the noncollinear angle does not appear in the wave-vector approach.

The spatial variation of the pump-beam amplitude can also affect the OPA phase. Figure 1 shows the OPA phase variation with respect to pump intensity using the more-accurate OPA phase expression in Eq. (17) of Ref. 15. Equation (4) is not accurate enough at pump intensities below what is required for depletion or at comparable signal and pump intensities. These plots were

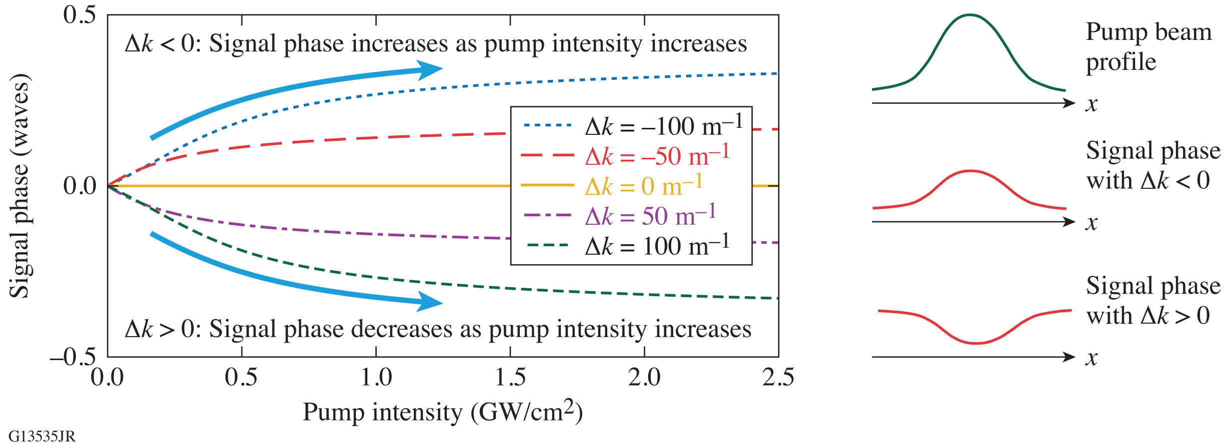

Figure 1
Effect of pump-beam intensity on the signal phase at different wave-vector mismatches.

generated using a 1-MW/cm^2 signal at 920 nm and a pump intensity at 527 nm from 0 GW/cm^2 to its depletion intensity, which is 2.5 GW/cm^2 for a 52-mm-long crystal. Unlike the phase effect, the amplitude effect depends on the sign of Δk. With positive Δk, the signal phase decreases with increasing pump intensity, whereas the trend is the opposite for negative Δk. When the phase mismatch is not equal to 0, the pump-beam shape is imprinted onto the signal phase. This qualitative behavior is illustrated on the right-hand side of Fig. 1 for a Gaussian-like pump beam.

It is interesting to note that this is similar to the intensity-dependent nonlinear effect with a sign dependency on phase matching as in cascaded nonlinearity.[15,16] The sign and amplitude change for spectral variations in Δk implies chromatic aberrations depend on the way Δk varies across the spectrum. Wang *et al.* described the chromatic effects in more detail.[17] With the linear dependence of Δk on frequency and a Gaussian-profile pump beam, this results in a radial group delay. The relative strength of the dispersion terms of Δk can easily change, depending on the phase-matching conditions and may exhibit more-complicated spatiotemporal coupling. On the other hand, chromatic effects induced by the pump phase are not significant because the signal phase's response is linear with the same slope wherever Δk is within the amplification bandwidth.

We conducted experiments to verify the prediction of pump wavefront and amplitude effect on the OPA phase in the final amplifier of the MTW-OPAL laser. Details about the MTW-OPAL system and the final pump laser are provided in Refs. 4 and 18. We specifically study the pump phase's effect in a collinear amplification geometry and the pump amplitude's effect. The amplifier, called NOPA5 being the fifth noncollinear OPA in the system, is based on a 52-mm-long, 70%-deuterated KDP crystal. The pump-signal angle for an optimum amplification bandwidth depends on the deuteration level.[19] The amplifier is currently configured in a collinear geometry because this configuration is optimal for the 70% DKDP crystal. The seed beam is a 100-mJ, 42-mm square beam. The seed pulse has a 150-nm bandwidth stretched to 1.2 ns. The pump beam is a 50-J, 40-mm square beam with a 1.7-ns pulse width. Beam size, pulse width, and bandwidth are estimated at 20% of the peak. The pump and signal are combined with a broadband dichroic mirror. The input pump wavefront and the output signal wavefront were sampled through leaky mirrors and measured with wavefront sensors after down-collimation and imaging. The signal wavefront was measured with a 930-nm bandpass filter. The inherent aberrations in the signal beam imaging system are estimated to be 0.16 waves peak to valley (p–v) based on a double-pass retro measurement. The design aberrations in the pump beam's imaging system are 0.2 waves p–v but no special effort was taken to measure the pump beam's diagnostic aberrations. The spectra of the input and output pulses are sampled by fiber-coupled diffusers and transported to a multichannel spectrometer. The energies of the pump and signal pulses are either measured directly with calorimeters or indirectly in the diagnostics beam path with calibration factors. The crystal is angle tuned using a precision rotation stage. We induce specific phase modulations on the pump beam using a phase plate after the main pump amplifiers or specific amplitude modulation upstream before the amplifiers using a programmable beam-shaping system.[20]

A high-order phase plate with ~2.5 waves (p–v) transmitted wavefront at 526 nm was inserted in the pump-beam path to introduce a more-complex phase profile, as shown in Fig. 2(a). The resulting signal intensity and wavefront, with bandpass filtration at 930 nm, are shown in Fig. 2(b); the calculated counterparts are shown in Fig. 2(c). The measured wavefront is a relative wavefront referenced against the amplified signal wavefront without the phase plate. The amplitude and overall shape of the measured and calculated wavefronts, in particular local extrema, are in excellent agreement.

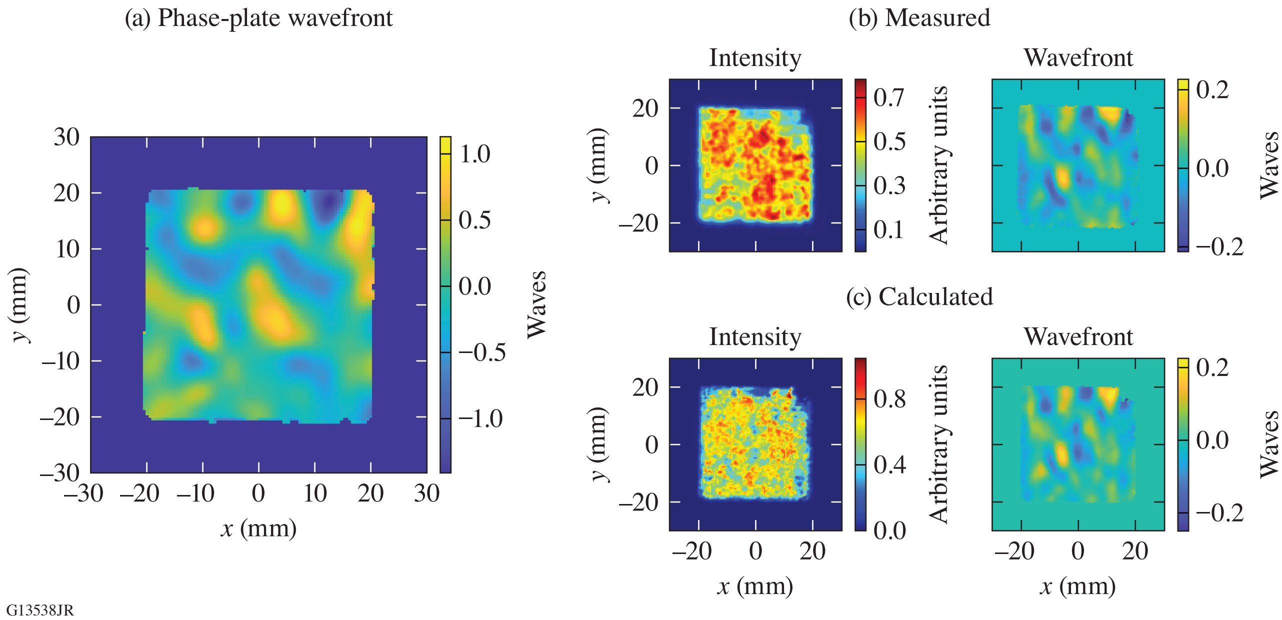

Figure 2
(a) Transmitted wavefront of the phase plate, (b) measured intensity and wavefront, and (c) calculated intensity and wavefront at 930 nm.

To investigate the amplitude effect, the beam-shaping system[20] for the pump beam was used to produce a cylindrical Gaussian-like beam as shown in Fig. 3(a). The crystal angle was detuned $\pm 0.017°$ to change the sign of Δk and demonstrate its sign sensitivity on the induced wavefront. The lineouts of the measured and calculated wavefronts at 930 nm are shown in Fig. 3(b) as solid and dashed lines, as shown in the legend. The lineouts are averaged over 80% of the central region of the beam in the y direction. This comparison shows a good agreement in the overall quadratic shape following from the pump-beam profile. We also measured the wavefronts at three wavelengths (890 nm, 930 nm, and 990 nm) using bandpass filters installed in front of three separate wavefront sensors as shown in Fig. 3(c), which directly show chromatic effect.

We presented a detailed theory of the OPA phase produced by the pump and signal wavefronts and measured the OPA phase from the pump wavefront. The main theoretical result is that the OPA phase is proportional to the derivative of the pump and signal wavefronts in the phase-matching direction. The birefringent walk-off and noncollinear interaction geometry couple the phase derivative terms to phase mismatch and therefore to the OPA phase. The effect of the pump-beam profile has also been investigated. Our expressions showed the OPA phase depends on the pump intensity and the sign of the phase mismatch. The signal wavefront modulation caused by the pump-intensity modulation is more sensitive at a lower pump intensity. A small amount of chromatic aberrations following the shape of the pump profile is expected.

We performed experiments demonstrating both the phase and amplitude effect of the pump beam on the OPA phase using a broadband OPA amplifier in a collinear geometry. The pump wavefront effect was investigated by adding a high-order phase plate in the pump beam. The experiment confirmed that the induced signal phase is related to the pump phase gradient in the phase-matching direction. The OPA phase due to the pump beam profile was measured for different phase-matching conditions

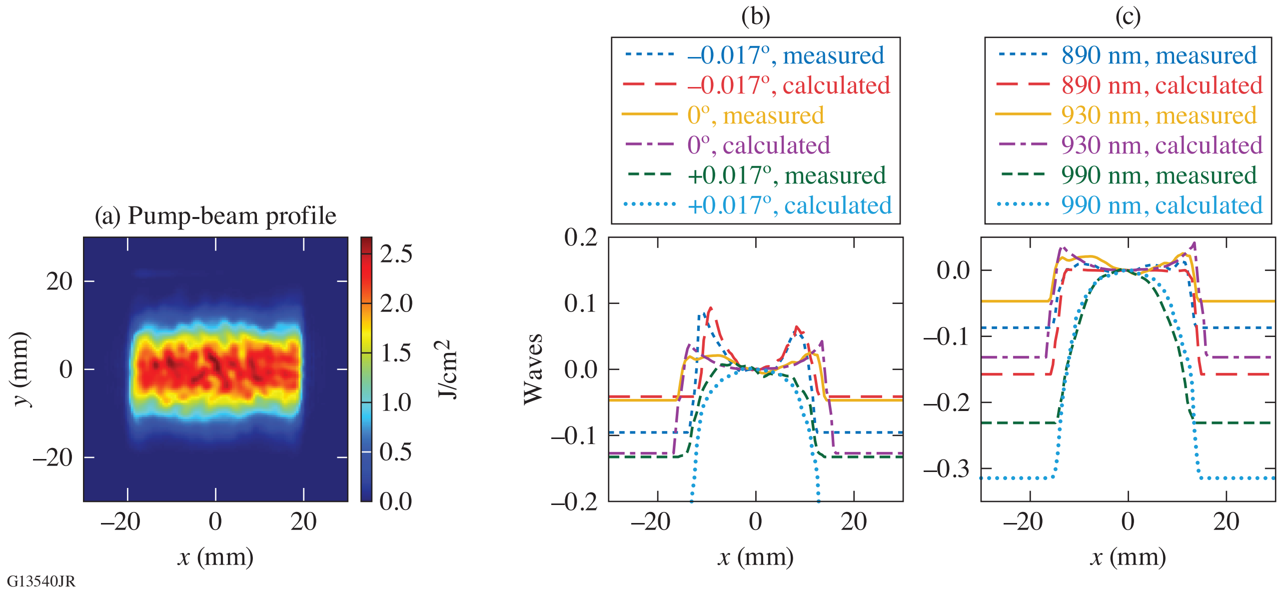

Figure 3
(a) Vertically nonuniform pump-beam profile; (b) measured and calculated wavefront-averaged vertical lineouts at different crystal tuning angles; (c) measured and calculated wavefront averaged lineouts at three wavelengths at 0°.

obtained by slightly detuning the crystal. The measurements confirmed that the amplitude-induced OPA phase depends on the sign of the phase mismatch and the pump-beam profile.

The traditional understanding of the general behavior of the pump-beam wavefront being transferred to the idler beam is, in general, correct in the sense that the OPA phase introduced by the pump-beam wavefront is generally an order of magnitude smaller than the pump wavefront directly transferred to the idler beam. The transfer to the signal beam can be non-negligible, however, for a larger system with large wavefront errors. The experimental verification of the pump and signal phase effect for noncollinear geometry will be discussed in subsequent publications. We expect the considerations presented in this summary will play an important role for future construction of a scaled-up high-energy broadband OPCPA system, where the wavefront becomes difficult to control as the beam size increases.

This material is based upon work supported by the Department of Energy National Nuclear Security Administration under Award Number DE-NA0003856, the University of Rochester, and the New York State Energy Research and Development Authority.

1. G. A. Mourou, T. Tajima, and S. V. Bulanov, Rev. Mod. Phys. **78**, 309 (2006).
2. C. N. Danson *et al.*, High Power Laser Sci. Eng. **7**, e54 (2019).
3. V. V. Lozhkarev *et al.*, Opt. Express **14**, 446 (2006).
4. J. Bromage *et al.*, High Power Laser Sci. Eng. **9**, e63 (2021).
5. L. Xu *et al.*, Opt. Lett. **38**, 4837 (2013).
6. M. Galletti *et al.*, High Power Laser Sci. Eng. **8**, e31 (2020).
7. S. Yang *et al.*, Opt. Express **28**, 11,645 (2020).
8. R. S. Nagymihaly *et al.*, Opt. Express **27**, 1226 (2019).
9. I. N. Ross *et al.*, J. Opt. Soc. Am. B **19**, 2945 (2002).
10. W. Li *et al.*, Appl. Phys. B **123**, 37 (2016).
11. X. Wei *et al.*, Opt. Express **16**, 8904 (2008).
12. P. Yuan *et al.*, High Power Laser Sci. Eng. **2**, e30 (2014).
13. Y. Chen *et al.*, Adv. Condens. Matter Phys. **2018**, 5731938 (2018).

14. H. J. Bakker *et al*., Phys. Rev. A **42**, 4085 (1990).
15. S. W. Bahk, Opt. Lett. **46**, 5368 (2021).
16. R. DeSalvo *et al*., Opt. Lett. **17**, 28 (1992).
17. Y. Wang *et al*., Opt. Lett. **46**, 5743 (2021).
18. I. A. Begishev *et al*., Appl. Opt. **60**, 11,104 (2021).
19. K. Ogawa *et al*., Opt. Express **17**, 7744 (2009).
20. S.-W. Bahk, I. A. Begishev, and J. D. Zuegel, Opt. Commun. **333**, 45 (2014).